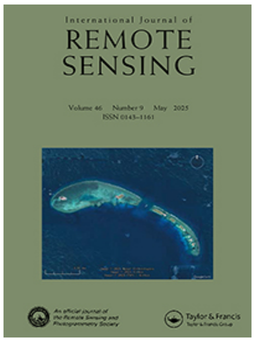

International Journal of Remote Sensing

ISSN: 0143-1161 (Print) 1366-5901 (Online) Journal homepage: www.tandfonline.com/journals/tres20

Sensitivity analysis of the Green Shoulder indices in pre-emergence detection of single trees attacked by European spruce bark beetle

Langning Huo, Niko Koivumäki, Roope Näsi & Eija Honkavaara

To cite this article: Langning Huo, Niko Koivumäki, Roope Näsi & Eija Honkavaara (2025) Sensitivity analysis of the Green Shoulder indices in pre-emergence detection of single trees attacked by European spruce bark beetle, International Journal of Remote Sensing, 46:9, 3513-3525, DOI: 10.1080/01431161.2025.2482747

To link to this article: https://doi.org/10.1080/01431161.2025.2482747

Published online: 28 Mar 2025.

INTERNATIONAL JOURNAL OF REMOTE SENSING
2025, VOL. 46, NO. 9, 3513–3525
https://doi.org/10.1080/01431161.2025.2482747

Taylor & Francis
Taylor & Francis Group

OPEN ACCESS Check for updates

Sensitivity analysis of the Green Shoulder indices in pre-emergence detection of single trees attacked by European spruce bark beetle

Langning Huo[a], Niko Koivumäki[b], Roope Näsi[b] and Eija Honkavaara[b]

[a]Department of Forest Resource Management, Swedish University of Agricultural Sciences, Umea, Sweden; [b]Department of Remote Sensing and Photogrammetry, Finnish Geospatial Research Institute, National Land Survey of Finland (NLS), Espoo, Finland

ABSTRACT

The application of hyperspectral cameras for forest health monitoring enables precise detection of stress-related changes in vegetation, such as those caused by spruce bark beetle infestations. In a previous study, Green Shoulder Indices (GSIs) were proposed, which exhibited high capacities to indicate trees with decreasing vitality caused by spruce bark beetle infestation using hyperspectral drone images. However, the detection accuracy of these indices may be influenced by the selection of various parameters. This study conducts a sensitivity analysis of the indices and aims to assess how the detection accuracy is impacted by different parameter choices. The detectability obtained from the GSIs was calculated and compared when (1) using the brightest or centremost pixels from the crown segments with different thresholds, (2) smoothing the spectral curves with different levels, and (3) using bands with varying bandwidths. The results showed that the GSIs were not sensitive to whether the brightest or centremost pixels were used for detection. Stronger smoothing caused the derivative peak at 545 nm to shift towards smaller wavelengths when a tree was under increasing stress, but the detectability obtained using GSIs did not decrease with stronger smoothing. The simplified GSIs using three wide spectral bands centred at 490 nm, 530 nm, and 550 nm (MS GSIs) slightly decreased the detection accuracy compared to narrowband MS GSIs, but the differences were minor, e.g. decreased from 0.86 to 0.80 using the index with the highest detectability ($\delta GSCR1_{MS}$). This study highlights the robustness of GSIs against tested factors and implies their potential for forest stress monitoring and damage control.

ARTICLE HISTORY
Received 5 December 2024
Accepted 17 March 2025

KEYWORDS
European spruce bark beetle; early detection; remote sensing; hyperspectral imagery; drone imagery

1. Introduction

The European spruce bark beetle (*I. typographus*) is one of the most devastating forest pests in Europe, which has significantly increased the mortality of Norway spruce (Köhl, Linser, and Prins 2020). Detecting infested trees and removing them from forests

CONTACT Langning Huo langning.huo@slu.se Department of Forest Resource Management, Swedish University of Agricultural Sciences, Umea 90 183, Sweden

before a new generation of bark beetle emerges is important for damage control. Among the studies achieving early detection before brood emergence, Huo, Koivumäki, et al. (2024) used hyperspectral drone images and proposed to use features in the green shoulder region (490–550 nm) to form Green Shoulder Indices (GSIs, Figure 1). Two types of indices were proposed, one using values from the first and second derivative curves, requiring hyperspectral data to calculate (denoted as Hyperspectral Green Shoulder Indices, HS GSIs, (Equations 1, 2) and the other type is simplified indices, which only require reflectance from three bands to calculate (denoted as Multispectral Green Shoulder Indices, MS GSIs, (Eq. 3, 4) Although improved detection with higher accuracy was presented when using HS GSIs and MS GSIs, some factors need to be further analysed to test the robustness of the new methodology.

1.1. Pixel selection strategy

It is essential to assess whether the detection performance is sensitive to crown segmentation and pixel selection strategy. Calculating crown reflectance has been regarded as a basic step for spectral analysis. After obtaining the crown segments, different crown pixel selection strategies include (1) using pixels from the entire crown (Einzmann et al. 2021; Huo, Lindberg, et al. 2023; Huo, Koivumäki, et al. 2024), (2) using pixels within a certain radius to the crown centre, e.g. 0.5 m (Klouček et al. 2019; Näsi et al. 2015) and 1 m (Näsi et al. 2018), and (3) using the brightest pixels (Bozzini et al. 2024), e.g. 20% brightest pixels (Cessna et al. 2021) and 50% brightest pixels (Bárta et al. 2022). While different methods and parameters have been used in different studies, very few have analyzed how much the crown pixel selection affected early detection of infested trees.

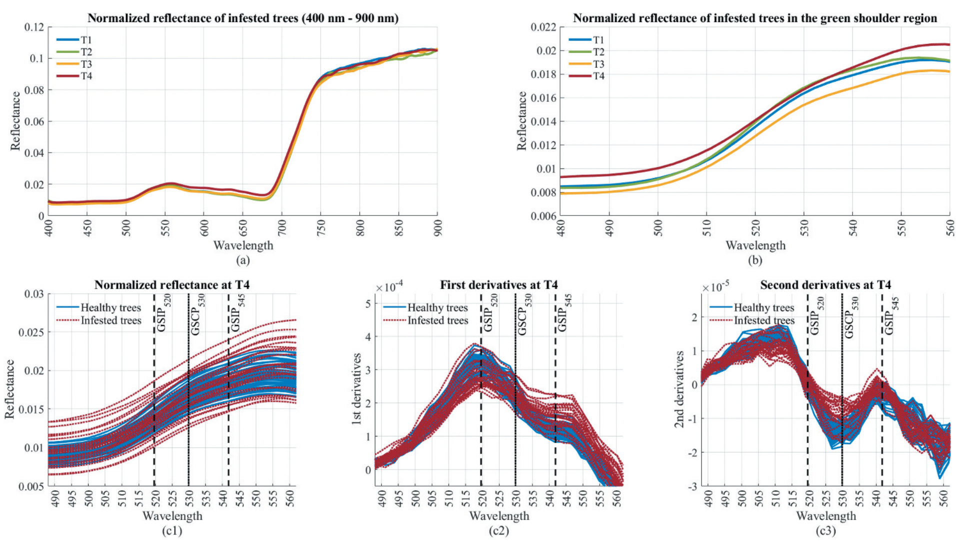

Figure 1. Averaged spectral curves of infested trees at four times T1, T2, T3, and T4 at the VNIR (a) and green shoulder region (b), and the reflectance (c1), first and second derivative (c2, c3) of healthy and infested trees at T4.

Näsi et al. (2018) discovered that using the average of the three or six brightest pixels (0.10 m or 0.12 m resolution) obtained higher spectral separability between healthy and infested trees than using all crown pixels. Huo, Yu, et al. (2024) compared the pixel selection strategy of using different thresholds to select the brightest or centermost pixels. They found that using the brightest pixels (>80% percentile) or centremost pixels (e.g. 0.5 m radius) in the tree crowns had higher detectability than using all pixels for early-infested-tree detection, but not for trees in later stages of infestation.

1.2. Smoothing effect

The proposed HS GSIs in Huo, Koivumäki, et al. (2024) were calculated from derivative curves, which can be affected by hyperspectral smoothing, a step to minimize noise. While many vegetation-indices-based methods do not often apply spectral smoothing (Bárta et al. 2022; Honkavaara et al. 2020), it is a crucial step for derivative analysis, using smoothers such as Whittaker Smoother (Einzmann et al. 2021) and Savitzky-Golay (Huo, Yu, et al. 2024). However, smoothing can also change informative spectral features, e.g. causing shift effects of the peak or valley point in the derivative curves and causing a loss of spectral detail (Tsai and Philpot 1998). Therefore, it is important to understand how the spectral features in the green shoulder region shift with different smoothing levels and test whether the higher detection rates yielded by HS GSIs require a specific smoothing setting.

1.3. Robustness against bigger bandwidth

MS GSIs were proposed by Huo, Koivumäki, et al. (2024) as a simplified version of HS GSIs that only need reflectance from three bands, i.e. the Blue band at 490 nm, the Green band at 550 nm, and the Green Shoulder band at 530 nm. MS GSIs were intended for multispectral sensors, which can be much more cost-efficient than hyperspectral sensors and thus can cover larger areas without sacrificing spatial resolution. Nevertheless, the tested performance in Huo, Koivumäki, et al. (2024) still used reflectance from narrow bands (5.5 nm of Full-Width-Half-Maximum, FWHM), while multispectral sensors usually have channels with larger bandwidths. Therefore, this study aims to present how bigger bandwidths affect the detection. We will test whether the MS GSIs perform worse with larger bandwidths that are commonly used by multispectral sensors, e.g. 66 nm and 36 nm for the Blue and Green bands in Sentinel-2 images (Huo, Persson, and Lindberg 2021) and drone-based MAIA S2 multispectral camera (SAL Engineering S.R.L. and TIS S.R.L, Italy) (Huo, Koivumäki, et al. 2024), and 50 nm and 36 nm for the Blue and Green bands in PlanetScope images.

This study focuses on the sensitivity analysis of the GSIs proposed in Huo, Koivumäki, et al. (2024). We used the same dataset and parameters to quantify the detectability of infestations except for three steps: pixel selection, spectral smoothing, and different bandwidths for GSIs calculation. The aim is to present the robustness of the GSIs against those factors and potential factors affecting the detection performance, which are crucial to consider before implementing the method for practical monitoring and management of forest damage caused by bark beetles.

Table 1. Hyperspectral AFX10 camera settings during the flights.

Camera setting			
Spatial: Binning; pixels	1; 1024	Flight speed (m/s)	7
Spectral: Binning; bands	2; 224	Flight height (m)	100
FPS; Exposure time (ms)	71.72; 13.69	GSD (cm): tree tops, ground	5.6, 7
Flight details			
Date and UTC Time*	Illumination conditions	Sun zenith	Sun azimuth
26 July 2021 08:00–08:11	Sunny (uniform)	48°	131°
09 August 2021 10:10–10:25	Cloudy (quite uniform)	45°	175°
23 August 2021 08:49–09:00	Varying	52°	150°
07 September 2021 10:03–10:12	Sunny (uniform)	54°	175°

*Local time was UTC +03 hours.

2. Materials and methods

2.1. Test area and reference data

The test area was located in Helsinki city central park (60°15′25.200″N, 24°55′19.200″E). A 20 ha area dominated by mature Norway spruce trees with ongoing infestation by *I. typographus* was selected for the study. In 2021, 56 healthy and 41 infested trees were selected as the samples. The healthy trees were selected based on a field survey conducted on 6–9 September 2021 to determine whether the trees were healthy without any attack symptoms. The infested trees were selected from visual interpretation of RGB orthophotos acquired on 7 September 2021 and 21 June 2022. Trees with green tree crowns on 7 September 2021 and appeared dead on 21 June 2022 were determined as attacked by the first filial generation (F1) while still in the green-attack phase of the infestation.

2.2. Remote sensing datasets

The DJI Matrice M600 hexacopter drone was employed as the platform for the pushbroom hyperspectral camera, Specim AFX10 VNIR. The AFX10 camera, weighing 2.1 kg, was mounted on a Gremzy T7 gimbal. The camera had an integrated computer and a high-end GNSS/IMU unit, and had a 15 mm focal length and spectral sensitivity of 400–1000 nm. With a spectral binning of 2 and spatial binning of 1, it achieved a spectral resolution of 5.5 nm, a spectral sampling interval of 2.68 nm, 224 spectral bands, and 1024 spatial pixels (Specim, 2022). Details of the camera settings are given in Table 1.

Hyperspectral VNIR images were collected at two-week intervals, denoted as T1, T2, T3, and T4, from the beginning of the bark beetle attack to the brood emergence of the next bark beetle generation (pre-emergence period), and infested trees started to experience increasing stress and vitality decline at some point during this time. The drone flights were done from approximately 100 m above ground level, and the side overlaps of flight lines were 36% at ground level and 20% at treetops. The camera settings and flight conditions are listed in Table 1.

The hyperspectral datasets were georectified using the Specim CaliGeoPRO v2.3.12 software. The post-processed kinematic (PPK) GNSS/IMU solutions were calculated using the Applanix PosUAV v 8.6 software for the flight trajectories. The raw image pixel values of AFX datasets were transformed to the units of radiance using the Specim CaliGeoPRO v2.3.12 software, and georectification was carried out with a digital surface model (DSM) of 1 m GSD (Ground Sample Distance) smoothed with a Gaussian filter. The radiance images were transformed to reflectances using panels with 25% nominal reflectance.

This study used the same hyperspectral VNIR data as Huo, Koivumäki, et al. (2024), and more details can be seen in Huo, Koivumäki, et al. (2024).

2.3. Tree segmentation

Tree crowns were automatically segmented using a marker-controlled watershed algorithm, the same as presented in Huo, Koivumäki, et al. (2024). A single-band image (wavelengths at 553 nm) was first used to make a segmentation mask, which was then applied to every band. To make the segmentation mask, pixels with the maximum pixel values from a smoothed single-band image were used as the markers, and then a marker-controlled watershed segmentation was conducted using the SegmentTrees tool in the Lidar Toolbox in Matlab (MathWorks, Inc., 2021). Shadow or gap pixels were excluded from the segments if the reflectance from the green band was lower than 0.015 (Huo et al. 2023; Huo, Koivumäki, et al. 2024). After these steps, images of individual tree crowns were derived with the markers as the tree tops. Then, health status of the trees shown in each image was determined by matching the markers with the location of the reference data. Among all segments, 47 healthy and 29 infested trees were successfully segmented from all images acquired from T1 to T4 (Please see Huo, Koivumäki, et al. 2024 for a full segmentation description.).

2.4. Green shoulder indices

The reflectance of each tree was calculated by averaging certain pixel values from the crown pixels (more details in Section 2.2). To match the spectrum from different times, the spectra were all normalized by the Frobenius norm, which is the square root of the sum of squares of reflectance values in the full spectra. The spectral curves were also smoothed by Savitzky-Golay smoothing with polynomial order 2 and frame length 7 (more details in Section 2.3). The calculation of Green Shoulder Points is listed in Table 2. Hyperspectral Green Shoulder Indices (HS GSIs) and simplified Green Shoulder Indices (MS GSIs) were calculated by Equations 1-4.

Table 2. Abbreviation and calculation of the green shoulder points.

Abbr.	Term	Calculation
GSIP	Green Shoulder Inflection Point	The point of maximum slope on the reflectance spectrum in the green shoulder range (490–550 nm), where the 1st derivatives show peak values at approx. 520 nm and 545 nm.
$GSIP_{520}$	1st derivative of GSIP at approx. 520 nm	
$GSIP_{545}$	1st derivative of GSIP at approx. 545 nm	
GSCP	Green Shoulder Curvature Point	The point of maximum curvature on the reflectance spectrum in the green shoulder range (490–550 nm), where the 2nd derivatives show valley values at approx. 530 nm.
$GSCP_{530}$	2nd derivative of GSCP at approx. 530 nm	

$$\text{Green Shoulder Curvature Ratio 1 } GSCR1 = \frac{\mathrm{GSIP}_{545}}{-\mathrm{GSCP}_{530}} \tag{1}$$

$$\text{Green Shoulder Curvature Ratio 2 } GSCR2 = \frac{\mathrm{GSIP}_{545}}{\mathrm{GSIP}_{520} \times (-\mathrm{GSCP}_{530})} \tag{2}$$

$$GSCR1_{MS} = \frac{R_{550} - R_{530}}{R_{530} - \frac{R_{550}+R_{490}}{2}} \tag{3}$$

$$GSCR2_{MS} = \frac{R_{550} - R_{530}}{(R_{530} - R_{490}) \times \left(R_{530} - \frac{R_{550}+R_{490}}{2}\right)} \tag{4}$$

To show the vitality changes over time and to normalize the indices with the initial status of trees, we also normalized the indices by comparing them to the first image acquired at T1, as

$$\delta VI = \left| \frac{(VI_{Ti} - VI_{T1})}{VI_{T1}} \right| \tag{5}$$

where VI refers to the tested indices GSIP_{545}, GSCP_{530}, GSCR1, GSCR2, $GSCR1_{MS}$, $GSCR2_{MS}$ and Ti refers to the image acquired at T1, T2, T3, and T4. These four tested indices should be stable for healthy trees over time while increasing with longer durations of the infestation.

2.5. Detection evaluation

The detection performance of early infestation using green shoulder indices was evaluated in the same way as Huo, Koivumäki, et al. (2024) to make the results comparable. The performance was quantified by detectability, i.e. detection rate, calculated using images from all acquisitions T1 + T2 + T3 + T4. We first calculated the 1% or 99% percentile of the indices values for the healthy trees at all times T1 to T4, and defined the range as a 'healthy range'. Among the infested trees, the ones with index values outside this range were considered detectable, and the proportion of them was treated as 'detectability'. Detectability represented how well the infested trees could be identified by unsupervised classification, e.g. using empirical thresholds.

2.6. Sensitivity analysis

The study tested the robustness of green shoulder indices in changing parameters in three steps.

(1) Pixel selection strategy: selecting pixels in the crown segments to calculate the crown reflectance. This study tested two ways of averaging crown reflectances. (i) averaging the brightest 5%, 10%, 15%, 20%, 25%, 50%, 75%, and 90% pixels, and (ii) averaging the pixels that were within 0.1, 0.25, 0.5, . . ., 3.5 m radius from the crown top.

(2) Smoothing effect: denoising the spectral curves using different frame lengths. Smoothing algorithms are often used to process the spectral curves to reduce noise, but smoothing can often slightly change the signature properties and influence the performance of derivatives and indices. Therefore, we tested how the Green Shoulder Inflection Points and Green Shoulder Curvature Points shifted when using different frame lengths of the Savitzky-Golay smoothing from 3 to 15, with larger values making the curves smoother. Then HS GSIs and MS GSIs were calculated and tested to determine whether the detectability was stable when using different smoothing parameters.

(3) Robustness against different bandwidths: simulating reflectance acquired by multi-spectral sensors and testing the performance of MS GSIs. This involved computing the mean reflectance of bands from the hyperspectral images within bandwidths ranging from 5 nm to 70 nm. Detection was evaluated using the same method above when using $GSCR1_{MS}$, $GSCR2_{MS}$, $\delta GSCR1_{MS}$ and $\delta GSCR2_{MS}$ with changing bandwidths.

3. Results

3.1. Pixel selection strategy

Overall, the detectability results indicated that infested trees could not be detected at T1 and T2 (1–5 weeks after attacks), but detection rates began to increase thereafter (Figure 2, Figure 1). After segmentation, we explored which pixels in the tree crown were more sensitive to infestation. We first tested whether using only the brightest pixels could improve early identification. In general, most GSIs did not show increasing or decreasing trends of changing the detectability when using brighter pixels, especially not at T4 (Figure 2b). Some GSIs showed slightly lower detectability at T3 (Figure 2b) when averaging with too dark pixels (more than 75% brightest pixels) or only averaging too brightest pixels (less than 25% brightest pixels). When averaging pixels within specific radii of the tree tops, most VIs yielded lower accuracy with radii smaller than 1.75 m at T3 and 1 m at T4 (Figure 2b). Detectability obtained from larger

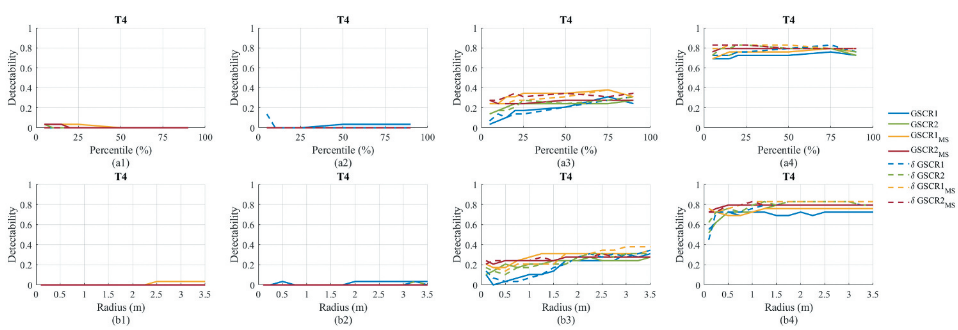

Figure 2. Detectability of VIs using the brightest pixels above different percentiles (a) and different radii (b) of the tree segments to average reflectance of individual tree crowns, using images from T1, T2, T3, and T4. The solid lines are the detectability using VIs, and the dash lines are the detectability using the normalized VIs (δVI).

radii than those mentioned thresholds were very similar. MS GSIs were more robust against changing pixel selection. In the following steps, we continued the analysis with crown reflectance averaged from 75% of the brightest pixels without radius limitation. Note that the crown segments were still used in this step. For example, if a tree had a crown radius smaller than 3 m, only the crown pixels were averaged without ground pixels or shadows within this range.

3.2. Smoothing effect

With a longer time of being infested, the infested trees showed larger values at $GSIP_{545}$ and $GSCP_{530}$ than the healthy trees, while the differences in $GSIP_{520}$ values were not pronounced. We tested how $GSIP_{545}$, $GSIP_{520}$ and $GSCP_{530}$ shifted when using different frame lengths of the Savitzky-Golay smoothing from 3 to 15, with larger values making the curves smoother. Results showed that $GSIP_{545}$ shifted towards smaller wavelengths when using frame lengths ≥11, and the larger the frame length used, the more shift $GSIP_{545}$ had (Figure 3(b)). $GSCP_{530}$ also shifted slightly to smaller wavelengths when using frame lengths of 15 (Figure 3(c)). When using frame lengths >15, the smoothing was so strong that the minor peak of the first derivative curve at 545 nm disappeared, so HS GSIs could not be calculated.

Figure 4 presents the influence of the smoothing technique on the detection accuracy. For HS GSIs, the detectability was relatively low when smoothing with a frame length of smaller than 5, but when the smoothing frame length was increased from 5 to 15, there was no clear trend in detectability, although some fluctuations appeared in T3 (Figure 4(a) dashed lines). For MS GSIs, the detectability differed very slightly between no smoothing and strong smoothing.

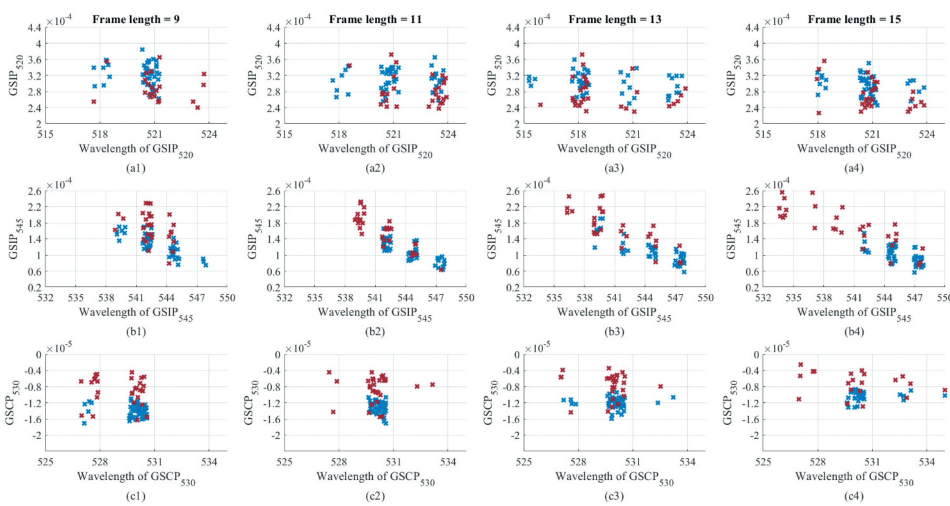

Figure 3. Distribution of GSIP520 (a), GSIP545 (b) and GSCP (c) Points of healthy (blue crosses) and infested (red crosses) trees with different frame lengths of 9 (1), 11 (2), 13 (3), and 15(4) for the spectral smoothing at T4.

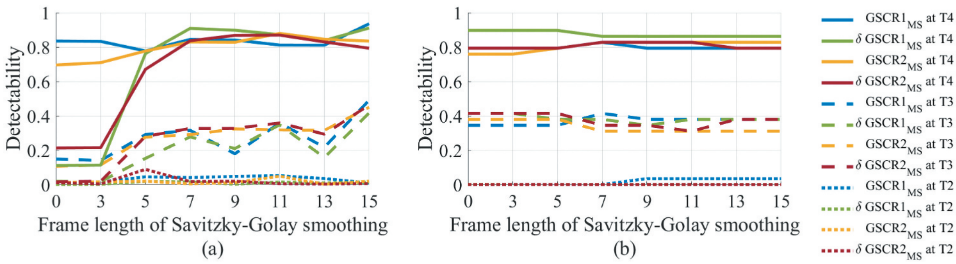

Figure 4. Detectability of HS GSIs (a) and MS GSIs (b) When using different smoothing parameters. Detectability at T4 (solid lines), T3 (dashed lines), and T2 (dotted lines) were all presented in the figures. A frame length of 0 represents the cases without smoothing.

3.3. Robustness against different bandwidths

Figure 5 presents the effects of varying the bandwidths when computing the MS GSIs. We first used the same bandwidths for all three bands, i.e. the Blue band at 490 nm, the Green Shoulder band at 530 nm, and the Green Peak band at 550 nm. We observed large decreases in detectability when bandwidths were larger than 60 nm (Figure 5(a)). We then fixed the bandwidth of 60 nm and 30 nm at the Blue and Green Peak bands, respectively, and changed the bandwidth of Green Shoulder band (Figure 5(b)). It did not show a decreasing effect on detectability with larger bandwidth. However, when the bandwidth of 60 nm was fixed at both Blue and Green Shoulder bands, the decreasing effect appeared with increasing bandwidths of Green Peak band (Figure 5(c)). This illustrated the importance of having a relatively narrow bandwidth at Green Peak band, but not at the Blue or Green Shoulder bands.

$GSCR1_{MS}$ and $\delta GSCR1_{MS}$ showed higher robustness against larger bandwidths than $\delta GSCR2_{MS}$ and $\delta GSCR2_{MS}$. $\delta GSCR1_{MS}$ had the best tolerance with larger bandwidths and only decreased the detectability at T4 from 0.86 to 0.80 when using a bandwidth of 60 nm

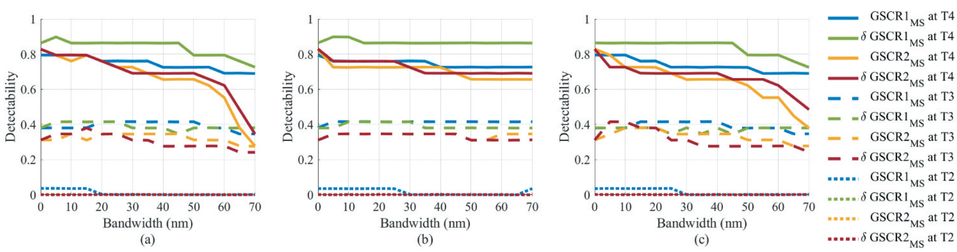

Figure 5. The detectability of MS GSIs changes with different bandwidths. (a) Changing bandwidths for all three bands. (b) Changing bandwidths of the Green Shoulder band while having a fixed bandwidth of 60 nm at the Blue and Green Peak bands. (c) Changing bandwidths of the Green Shoulder band while having a fixed bandwidth of 60 nm at the Blue and Green Shoulder bands. Detectability at T4 (solid lines), T3 (dashed lines), and T2 (dotted lines) were all presented in the figures, as the highest detectability shown at T4 around 0.6–0.9, medium detectability shown at T3 around 0.2–0.4, and low detectability close to 0 at T2. Bandwidth of 0 in the figures refers to the case when using reflectances from the original narrow bands.

for all three bands compared to narrowbands. When using bandwidths of 60 nm, 30 nm, and 30 nm at Blue, Green Shoulder, and Green Peak bands, a similar setting as the Plantescope images, the detectability was 0.76, 0.86, 0.73, and 0.73 at T4 using the four MS GSIs, i.e. $GSCR1_{MS}$, $\delta GSCR1_{MS}$, $GSCR2_{MS}$, and $\delta GSCR2_{MS}$, respectively. The detectability was slightly lower than narrow bands, i.e. 0.80, 0.86, 0.83, and 0.83 using the same four MS GSIs.

4. Discussion

This study presented the robustness of the GSIs when changing parameters in the spectral analysis, including pixel selection, smoothing effect, and different bandwidths. On the contrary to the results from two previous studies showing brightest pixels or centremost pixels could improve early detection (Huo, Yu, et al. 2024; Näsi et al. 2018), this study presented that the detectability was affected less by pixel selection when using green shoulder indices, especially GSCR2_{MS}. This study used the same method to segment tree crowns and the same parameters to select pixels as Huo, Yu, et al. (2024). Different camera types may cause the opposite results. The cameras used in this study were line scan cameras, while the other two studies (Huo, Yu, et al. 2024; Näsi et al. 2018) used frame cameras with pass filters that required accurate co-registration between bands and photometric stereo imaging systems and algorithms. As different light conditions, such as direct or diffuse, could influence the distribution of the reflectance within tree crowns, it is expected that using the brightest pixels under direct light could improve the detection, while it was not pronounced in this study. The results illustrated that whether using the brightest or centremost pixels improves early detection could be case-wise, and more studies are needed to explore whether differences were caused by different camera types.

This study also explored the shift effects of the Green Shoulder Points (GSPs, including GSIP_{520}, GSIP_{545}, and GSCP_{530}) from the stressed trees. Many studies have shown that Red Edge Point (REP) shifted to smaller wavelengths after plants got stressed and different methods were developed to estimate the wavelength of the REP to quantify plant stress (Li, Zhang et al. 2024; Li, Huo, and Zhang 2024). Our results showed that, when using smaller frame lengths of the Savitzky-Golay smoothing on the spectral curves, none of the GSPs showed a shift trend during infestation. However, GSIP_{545} shifted to smaller wavelengths when using bigger frame lengths, while the shifts of GSIP_{520} and GSCP_{530} were still very subtle. Moreover, the bigger frame lengths used, the more GSIP_{545} shifted after a longer infestation time. The shift effect under different smoothing parameters was consistent with a similar experiment in another study (Tsai and Philpot 1998).

The shift mechanism and calculation of REP and GSP have many similarities. They both shift when pigment contains change and they are both calculated by derivative analysis on the peak and valley values. The equation for GSCR1_{MS} (Equation 3) was similar to the linear 4-point interpolation of REP (Guyot and Baret 1988), but with 3-point interpolation instead. There have been different ways of calculating REP, e.g. the wavelengths with the maximum 1st derivative in the red-edge region (Dawson and Curran 1998), the linear 4-point interpolation method (Guyot and Baret 1988), the polynomial fitting method (Pu et al. 2003), the inverted Gaussian fitting method

(Bonham-Carter 1988), and the linear extrapolation method (Cho and Skidmore 2006). Some studies compared the performance and robustness of the REP using different calculation methods and found that the REP derived by the linear extrapolation method was more sensitive and robust to the plant nitrogen stress (Cho and Skidmore 2006; Main et al. 2011). Similar to REP, there should be different ways of calculating the GSP that can be further developed (Li et al. 2024).

This study also illustrated the robustness of MS GSIs against smoothing effects and wider bandwidths. While HS GSIs required certain smoothing levels to have stable performance (frame length of 7–15 of Savitzky-Golay smoothing), MS GSIs did not require smoothing to yield detectability similar to those after smoothing. Even with different smoothing levels, detectability barely changed with MS GSIs. MS GSIs were also relatively stable when bandwidth increased to 30 nm – 60 nm, similar to the bandwidths of Planetscope and Sentinel-2 images, and many drone-based multispectral cameras such as MAIA S2 (SAL Engineering S.R.L. and TIS S.R.L, Italy), DJI Mavic 3 M (SZ DJI Technology Co Ltd, China), and MicaSense Altum-PT (MicaSense, Inc, US). The results highlighted the big potential of the Green Shoulder band at 530 nm to be built in multispectral cameras and the potential to apply MS GSIs on images collected from small drones, airships, aircrafts, and satellites for large-area mapping.

5. Conclusions

This study contributes to the understanding of sensitivity and optimization of hyperspectral (HS) and multispectral (MS) Green Shoulder Indices (GSIs) for detecting trees infested by bark beetles before brood emergence. Through a sensitivity analysis, the study demonstrated that the GSIs were robust to variations in crown segmentation, spectral smoothing, and broader bandwidths. It was shown that using the brightest or centremost pixels in tree crowns was unnecessary for achieving optimal detectability. Additionally, while stronger spectral smoothing caused the derivative peaks at 545 nm to shift towards smaller wavelengths, it did not affect the detectability. Results also showed that wider bands on MS GSIs with 30–60 nm bandwidths slightly reduced the detectability compared to narrow bands, though the differences were minor. Among the tested GSIs, the parameters had a lower impact on the performance of MS GSIs than HS GSIs, demonstrating MS GSIs being effective and robust simplifications of HS GSIs. Normalization of index values from the first image further enhances robustness and accuracy compared to indices without normalization, e.g. $\delta GSCR1_{MS}$ against $GSCR1_{MS}$. A multispectral sensor for tree health monitoring is proposed with central wavelengths at 490 nm, 530 nm, and 550 nm with 10–30 nm bandwidths. Overall, this research highlights the potential of GSIs as a valuable tool for early vegetation stress monitoring and improves the understanding of the reliability of these indices under various conditions.

Disclosure statement

No potential conflict of interest was reported by the author(s).

Funding

The project is co-funded by the Swedish Governmental Agency for Innovation Systems Vinnova [project grant 2022-01218 to LH], the Forest Damage Center at the Swedish University of Agricultural Sciences [projects grant 260FDC57 and 260FDC44 to LH], the European Union with project RESDINET [projects grant 101078970 to LH and EH], and Academy of Finland [project grant 357380 to EH]. This study was affiliated with the Academy of Finland Flagship Forest–Human–Machine Interplay—Building Resilience, Redefining Value Networks and Enabling Meaningful Experiences [UNITE] [project grant 337127 to the Finnish Geospatial Research Institute.

Author contributions

Langning Huo: Conceptualization, Methodology, Validation, Formal analysis, Investigation, Writing – original draft, Writing – review & editing, Visualization, Project administration, Funding acquisition. Niko Koivumäki: Resources, Data curation, Writing – review & editing. Roope Näsi: Resources, Writing – review & editing. Eija Honkavaara: Conceptualization, Resources, Data curation, Writing – review & editing, Supervision, Project administration, Funding acquisition.

Data availability statement

No data is unavailable due to privacy.

References

Bárta, V., J. Hanuš, L. Dobrovolný, and L. Homolová. 2022. "Comparison of Field Survey and Remote Sensing Techniques for Detection of Bark Beetle-Infested Trees." *Forest Ecology & Management* 506 (1): 119984. https://doi.org/10.1016/j.foreco.2021.119984.

Bonham-Carter, G. F. 1988. "Numerical Procedures and Computer Program for Fitting an Inverted Gaussian Model to Vegetation Reflectance Data." *Computers & Geosciences* 14 (3): 339–356. https://doi.org/10.1016/0098-3004(88)90065-9.

Bozzini, A., S. Brugnaro, G. Morgante, G. Santoiemma, L. Deganutti, V. Finozzi, A. Battisti, and M. Faccoli. 2024. "Drone-Based Early Detection of Bark Beetle Infested Spruce Trees Differs in Endemic and Epidemic Populations." *Frontiers in Forests and Global Change* 7:87. https://doi.org/10.3389/ffgc.2024.1385687.

Cessna, J., M. G. Alonzo, A. C. Foster, and B. D. Cook. 2021. "Mapping Boreal Forest Spruce Beetle Health Status at the Individual Crown Scale Using Fused Spectral and Structural Data." *Forests* 12 (9): 1145. https://doi.org/10.3390/f12091145.

Cho, M. A., and A. K. Skidmore. 2006. "A New Technique for Extracting the Red Edge Position from Hyperspectral Data: The Linear Extrapolation Method." *Remote Sensing of Environment* 101 (2): 181–193. https://doi.org/10.1016/j.rse.2005.12.011.

Dawson, T. P., and P. J. Curran. 1998. "Technical Note a New Technique for Interpolating the Reflectance Red Edge Position." *International Journal of Remote Sensing* 19 (11): 2133–2139. https://doi.org/10.1080/014311698214910.

Einzmann, K., C. Atzberger, N. Pinnel, C. Glas, S. Böck, R. Seitz, and M. Immitzer. 2021. "Early Detection of Spruce Vitality Loss with Hyperspectral Data: Results of an Experimental Study in Bavaria, Germany." *Remote Sensing of Environment* 266 (1): 112676. https://doi.org/10.1016/j.rse.2021.112676.

Guyot, G., Baret, F. 1988. "Utilisation de la Haute Resolution Spectrale pour Suivre L'etat des Couverts Vegetaux". In *Spectral Signatures of Objects in Remote Sensing, Proceedings of the conference held 18-22 January, 1988 in Aussois (Modane), Francex*, edited by Guyenne, T.D., and J.J. Hunt. European Space Agency. 279.

Honkavaara, E., R. Näsi, R. Oliveira, N. Viljanen, J. Suomalainen, E. Khoramshahi, T. Hakala, et al. 2020. "Using Multitemporal Hyper- and Multispectral UAV Imaging for Detecting Bark Beetle Infestation on Norway Spruce." *International Archives of the Photogrammetry, Remote Sensing and Spatial Information Sciences* XLIII-B3-2020:429–434. https://doi.org/10.5194/isprs-archives-XLIII-B3-2020-429-2020.

Huo, L., N. Koivumäki, R. A. Oliveira, T. Hakala, L. Markelin, R. Näsi, J. Suomalainen, A. Polvivaara, S. Junttila, and E. Honkavaara. 2024. "Bark Beetle Pre-Emergence Detection Using Multi-Temporal Hyperspectral Drone Images: Green Shoulder Indices Can Indicate Subtle Tree Vitality Decline." *Isprs Journal of Photogrammetry & Remote Sensing* 216:200–216. https://doi.org/10.1016/j.isprsjprs.2024.07.027.

Huo, L., E. Lindberg, J. Bohlin, and H. J. Persson. 2023. "Assessing the Detectability of European Spruce Bark Beetle Green Attack in Multispectral Drone Images with High Spatial- and Temporal Resolutions." *Remote Sensing of Environment* 287 (2): 113484. https://doi.org/10.1016/j.rse.2023.113484.

Huo, L., H. J. Persson, and E. Lindberg. 2021. "Early Detection of Forest Stress from European Spruce Bark Beetle Attack, and a New Vegetation Index: Normalized Distance Red & SWIR (NDRS)." *Remote Sensing of Environment* 255 (7): 112240. https://doi.org/10.1016/j.rse.2020.112240.

Huo, L., R. Yu, E. Lindberg, H. J. Persson, J. Bohlin, and N. Li. 2024. "Influence of Crown Pixel Selection on the Early Detection of Bark Beetle Infestations Using Multispectral Drone Images." In *IGARSS 2024 - 2024 IEEE International Geoscience and Remote Sensing Symposium*, Athens, Greece. 5218–5221. IEEE.

Klouček, T., J. Komárek, P. Surový, K. Hrach, P. Janata, and B. Vašíček. 2019. "The Use of UAV Mounted Sensors for Precise Detection of Bark Beetle Infestation." *Remote Sensing* 11 (13): 1561. https://doi.org/10.3390/rs11131561.

Köhl, M., S. Linser, and K. Prins. 2020. "State of Europe's Forests 2020."

Li, N., L. Huo, and X. Zhang. 2024. "Using Only the Red-Edge Bands is Sufficient to Detect Tree Stress: A Case Study on the Early Detection of PWD Using Hyperspectral Drone Images." *Computers and Electronics in Agriculture* 217:108665. https://doi.org/10.1016/j.compag.2024.108665.

Li, N., X. Zhang, Z. Xie, and L. Huo. 2024. "Comparing Different Methods of Calculating Red-Edge and Blue-Edge Inflection Position from Hyperspectral Data to Early Detect Tree Disease." In *IGARSS 2024 - 2024 IEEE International Geoscience and Remote Sensing Symposium*, Athens, Greece. 10409–10412. https://doi.org/10.1109/IGARSS53475.2024.10642034.

Main, R., M. A. Cho, R. Mathieu, M. M. O'Kennedy, A. Ramoelo, and S. Koch. 2011. "An Investigation into Robust Spectral Indices for Leaf Chlorophyll Estimation." *Isprs Journal of Photogrammetry & Remote Sensing* 66 (6): 751–761. https://doi.org/10.1016/j.isprsjprs.2011.08.001.

MathWorks, I. 2022. *Optimization Toolbox Version: 9.4 (R2024b)*. Natick, Massachusetts, United States: The MathWorks Inc. https://www.mathworks.com.

Näsi, R., E. Honkavaara, M. Blomqvist, P. Lyytikäinen-Saarenmaa, T. Hakala, N. Viljanen, T. Kantola, and M. Holopainen. 2018. "Remote Sensing of Bark Beetle Damage in Urban Forests at Individual Tree Level Using a Novel Hyperspectral Camera from UAV and Aircraft." *Urban Forestry & Urban Greening* 30 (4): 72–83. https://doi.org/10.1016/j.ufug.2018.01.010.

Näsi, R., E. Honkavaara, P. Lyytikäinen-Saarenmaa, M. Blomqvist, P. Litkey, T. Hakala, N. Viljanen, T. Kantola, T. Tanhuanpää, and M. Holopainen. 2015. "Using UAV-Based Photogrammetry and Hyperspectral Imaging for Mapping Bark Beetle Damage at Tree-Level." *Remote Sensing* 7 (11): 15467–15493. https://doi.org/10.3390/rs71115467.

Pu, R., G. S. B. Peng Gong, M. R. Larrieu, and M. R. Larrieu. 2003. "Extraction of Red Edge Optical Parameters from Hyperion Data for Estimation of Forest Leaf Area Index." *IEEE Transactions on Geoscience & Remote Sensing* 41 (4): 916–921. https://doi.org/10.1109/TGRS.2003.813555.

Tsai, F., and W. Philpot. 1998. "Derivative Analysis of Hyperspectral Data." *Remote Sensing of Environment* 66 (1): 41–51. https://doi.org/10.1016/S0034-4257(98)00032-7.